Determination of the d31 piezoelectric coefficient of PbZrxTi1–xO3 thin films using multilayer buckled micromembranes

C. Ayela, Liviu Nicu, Caroline Soyer, Eric Cattan, C. Bergaud

Journal of Applied Physics

Determination of the d_{31} piezoelectric coefficient of $PbZr_xTi_{1-x}O_3$ thin films using multilayer buckled micromembranes

Cite as: J. Appl. Phys. **100**, 054908 (2006); https://doi.org/10.1063/1.2338139
Submitted: 07 February 2006 • Accepted: 24 June 2006 • Published Online: 12 September 2006

C. Ayela, L. Nicu, C. Soyer, et al.

AIP Publishing

Determination of the d_{31} piezoelectric coefficient of $PbZr_xTi_{1-x}O_3$ thin films using multilayer buckled micromembranes

C. Ayela[a] and L. Nicu
Laboratoire d'Analyse et d'Architecture des Systèmes, UPR 8001, 31077 Toulouse, France

C. Soyer and E. Cattan
Institut d'Electronique de Microélectronique et de Nanotechnologie, UMR 8520, 59046 Lille, France

C. Bergaud
Laboratory for Integrated Micro-Mechatronic Systems, UMI 2820 Tokyo 153-8505, Japan

(Received 7 February 2006; accepted 24 June 2006; published online 12 September 2006)

The aim of this paper consists in the determination of the piezoelectric transverse coefficient d_{31} of $PbZr_xTi_{1-x}O_3$ (PZT) thin films integrated in dedicated multilayer silicon-based micromembranes exhibiting an initial buckled profile. An analytical model specific to this configuration was built and used for the calculation of d_{31} starting with the static profiles of the microfabricated devices determined by means of a double-beam interferometer. The influence of dc voltage and buckling effects on the d_{31} piezoelectric coefficient at the microscale were investigated, and high values were obtained, from 30 to 75 pm/V, within a hysteresyslike cycle. These results demonstrated the good electrical behavior of PZT thin films at the microscale with a low influence of buckling effects and determined optimal operation conditions for high values of d_{31}. © *2006 American Institute of Physics*. [DOI: 10.1063/1.2338139]

I. INTRODUCTION

In recent years, thin piezoelectric films have widely addressed the development of various microdevices based on silicon technology with potential applications ranging from basic actuation (e.g., microfluidic pumps[1] or micromotors[2]) to physical[3] or biological sensing.[4] The common point consists of a micromachined membrane that stands for core mechanical element in the aforementioned applications. In most cases, the membrane is a stack of several thin films (including the piezoelectric one) with corresponding functions (generally a silicon substrate for the elastic foundation of the device, dielectrics—quite often silicon dioxide—for isolating the metallic layers from the silicon substrate, metals standing either as electrodes for the electrical activation of the piezoelectric material or active layer for biological grafting, etc.). Or, it is well known that by stacking thin films on a membranelike structure, if the resultant stress of the layers is compressive, one visible effect on the equilibrium position of the structure is a non-null out-of-plane initial static deflection (also known as buckling effect) that could dramatically affect the mechanical (and consequently, electrical) properties of the in-between piezoelectric film. It becomes thus of primary interest to theoretically and experimentally investigate the influence of the forced out-of-plane buckled equilibrium position of a membranelike multilayer structure on the piezoelectric coefficients of an in-between piezoelectric layer.

From the theoretical point of view, finite element modelization (FEM) is generally used in the microelectromechanical system (MEMS) design field. However, most of commercial FEM softwares do not take into account complex mechanical analysis such as buckling effects,[5] for instance. This is why the development of analytical models (when possible) is still a paved way for the MEMS structural design and optimization. Moreover, the perceived advantage of analytical models is the fact that the influence of the modification of one or more parameters to the global mechanical behavior can instantaneously be evaluated when compared to the effective run time of a FEM model. In the particular case of a multilayer buckled membrane integrating a piezoelectric layer, building a robust analytical model that predicts the quasistatic electromechanical behavior is strongly dependent not only on the knowledge of the mechanical parameters of all the materials but also of the piezoelectric coefficients of the piezoelectric layer.

When a piezoelectric thin film is clamped on a membranelike bender, the piezoelectric constants of interest are d_{31} and d_{33} (measured in pm/V). d_{31} represents the induced in-plane strain per unit electric field applied perpendicularly to the film plane while d_{33} stands for the induced strain perpendicular to the film plane per unit electric field applied in the same aforementioned direction. Even though for piezoelectric thin films belonging to the lead titanate zirconate (PZT) family it is well established[6] that the d_{33} value is about twice higher than d_{31}, the influence of the first one can be neglected in flexural actuation if several geometrical requirements are met (e.g., for circular-shaped actuators, the diameter of the piezoelectric patch clamped on one face is smaller than the one of the entire structure and the thickness of the piezoelectric film is comparable to the thickness of the global stack of layers forming the actuator). Several techniques for the determination of the d_{31} piezoelectric coefficient have been developed so far. Dubois and Muralt[7] or Cattan *et al.*[8] have characterized electrical charge generation with an external actuator on millimeter-sized cantilevers to determine an effective e_{31} (which is directly related to the d_{31} coeffi-

[a]Electronic mail: cayela@laas.fr

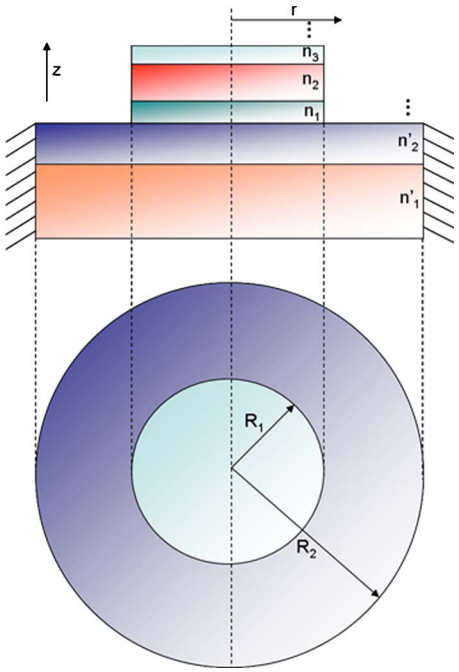

FIG. 1. (Color online) Cross section and top view of a multilayer clamped composite circular plate.

cient via the compliance coefficients of the piezoelectric film). As an alternative technique, Shepard *et al.*[9] used the wafer flexure technique in measuring charge generation on the entire wafer for the d_{31} calculation. Kanno *et al.*[10] came up with the d_{31} value by measuring the deflection of millimeter-sized cantilevers actuated by a PZT thin film. In the latter case, the deflection measurements were made by laser vibrometer coupled with laser interferometer.

The aim of this paper was to study the influence of a buckled equilibrium state of multilayer micromachined membranes on the piezoelectric constant d_{31} value. In particular, it was shown that the reduction of size from macro- to microscale and buckling effects of the structure do not affect the piezoelectric properties of PZT thin films. A representative analytical model was established to study the static behavior of multilayer piezoelectric buckled micromembanes. A measurement of static deflections for different constant actuation potentials was made using a dual-beam interferometer. The measurements were then implemented in a modified analytical model for the d_{31} calculation.

II. ANALYTICAL MODEL FOR PIEZOELECTRIC CIRCULAR PLATES WITH INITIAL STRESSES

The present model was established for a two part circular plate as shown in Fig. 1: an inner circular plate and an outer annular clamped plate. Each part contains different material layers, defined with properties such as their thickness and initial stress. The layers are bonded to one another with a stack radius of R_1 for the inner part and R_2 for the outer part. This composite is subjected to the resultant compressive or tensile initial stress N_0 and/or an applied voltage V across the piezoelectric thickness. The goal of the analytical model is first to determine the vertical deflection $w(r)$ of the composite, with respect to the initial conditions. Then, another interest is its generic behavior which allows the determination of one specific parameter if the other ones are known.

TABLE I. Nomenclature of parameters used in the analytical model.

Annotation	Signification
R_1 (μm)	Radius of the inner part
R_2 (μm)	Radius of the outer part
N_r (N/m)	Resultant radial force
N_θ (N/m)	Resultant circumferential force
u_0 (μm)	Radial displacement
θ (μm)	Circumferential displacement
w (μm)	Vertical deflection
Material properties	
E_i (GPa)	Young's modulus of the ith layer
ν_i	Poisson's ratio of the ith layer
σ_i (MPa)	Initial in-plane stress of the ith layer
h_i (μm)	Thickness of the ith layer
V (volt)	Transverse electric voltage applied on the piezoelectric layer

Wang *et al.*[5] have developed the same kind of model as the one described above for a bilayer plate. It is assumed that each layer is transversely isotropic, linearly elastic, and of constant thickness. As the layers' thicknesses are small compared to the radius, it is also assumed that the plate is in a state of plane stress normal to the z axis. All the annotations and material properties used in the model are summarized in Table I.

A. Mechanical approach for the model's development

The equilibrium equations for the symmetrical bending of a circular or annular plate under in-plane stress are determined by considering one element of the plate, conforming to Timoshenko and Krieger's hyptohesis.[11] These equations are given by

$$\frac{dN_r}{dr} + \frac{N_r - N_\theta}{r} = 0, \tag{1}$$

$$\frac{dM_r}{dr} + \frac{M_r - M_\theta}{r} = -N_r\theta, \tag{2}$$

where N_r and N_θ are the resultant forces along the radial and circumferential axes, respectively. M_r and M_θ are the corresponding moments. $-N_r\theta$ is the resultant shear force. The resultant forces and moments can be decomposed as $N_r = \tilde{N}_r + N_0$ and $M_r = \tilde{M}_r + M_0$, where $\tilde{N}_r$ and $\tilde{M}_r$ represent variations of the resultant force and moment different from those induced by N_0. N_0 represents the averaging value of the force due to the initial in-plane stress of all materials and is given by

$$N_0 = \sum_{i=1}^{n} \sigma_i h_i, \tag{3}$$

while M_0 is the corresponding bending moment exerted by N_0 at the interface between the annular and the circular regions of the structure.[5]

As $\tilde{N}_r$ is assumed to be small compared to N_0,[12] it is neglected in the expression for the resultant shear force. Equilibrium equations thus become

$$\frac{d\tilde{N}_r}{dr} + \frac{\tilde{N}_r - \tilde{N}_\theta}{r} = 0, \tag{4}$$

$$\frac{d\tilde{M}_r}{dr} + \frac{\tilde{M}_r - \tilde{M}_\theta}{r} = -N_0\theta. \tag{5}$$

As described by Prasad *et al.*,[13] the constitutive equations for a transversely isotropic, linearly elastic piezoelectric plate, related to the radial and circumferential strain displacement of Kirchoff's plate theory,[7] are given by

$$\begin{bmatrix} \tilde{\sigma}_{rr} \\ \tilde{\sigma}_{\theta\theta} \end{bmatrix} = [Qi]\left(\begin{bmatrix} \frac{du_0}{dr} \\ \frac{u_0}{r} \end{bmatrix} + z_i \begin{bmatrix} -\frac{d\theta}{dr} \\ -\frac{\theta}{r} \end{bmatrix} - \frac{V}{h_{\mathrm{PZT}}} \begin{bmatrix} d_{31} \\ d_{31} \end{bmatrix} \right), \tag{6}$$

where

$$[Q_i] = \frac{E_i}{1-\upsilon_i^2} \begin{bmatrix} 1 & \upsilon_i \\ \upsilon_i & 1 \end{bmatrix}. \tag{7}$$

z_i corresponds to the distance between the vertical position of a layer on the multilayer stack and the reference plane h_0 defined by[14]

$$h_0 = \frac{\Sigma_{i=1}^{n} \{[E_i/(1-\upsilon_i^2)]h_i[2(\Sigma_{j=1}^{i} h_j) - h_i]\}}{2\Sigma_{k=1}^{n}[E_k/(1-\upsilon_k^2)]h_k}. \tag{8}$$

The analytical expression for the resultant forces and moments is determined by integrating the constitutive equations through the total thickness of the multilayer plate, giving

$$\begin{bmatrix} \tilde{N}_r \\ \tilde{N}_\theta \end{bmatrix} = [A] \begin{bmatrix} \frac{du_0}{dr} \\ \frac{u_0}{r} \end{bmatrix} + [B] \begin{bmatrix} -\frac{d\theta}{dr} \\ -\frac{\theta}{r} \end{bmatrix} - \begin{bmatrix} N_r^p \\ N_\theta^p \end{bmatrix}, \tag{9}$$

and

$$\begin{bmatrix} \tilde{M}_r \\ \tilde{M}_\theta \end{bmatrix} = [B] \begin{bmatrix} \frac{du_0}{dr} \\ \frac{u_0}{r} \end{bmatrix} + [D] \begin{bmatrix} -\frac{d\theta}{dr} \\ -\frac{\theta}{r} \end{bmatrix} - \begin{bmatrix} M_r^p \\ M_\theta^p \end{bmatrix}, \tag{10}$$

where $[A] = \Sigma_{i=1}^{n} \int_{z_i}^{z_{i+1}} [Q_i] dz$ is the equivalent in-plane extensional stiffness matrix for the multilayer plate, $[B] = \Sigma_{i=1}^{n} \int_{z_i}^{z_{i+1}} [Q_i] z dz$ is the equivalent flexural-extensional coupling matrix, and $[D] = \Sigma_{i=1}^{n} \int_{z_i}^{z_{i+1}} [Q_i] z^2 dz$ is the equivalent flexural stiffness matrix. N_r^P and N_θ^P traduce the resultant flexural-extensional coupling forces induced by the piezoelectric layer for an applied voltage V and are given by

$$\begin{bmatrix} N_r^P \\ N_\theta^P \end{bmatrix} = \int_{z_{\mathrm{bottom\_PZT}}}^{z_{\mathrm{top\_PZT}}} \frac{V}{h_{\mathrm{PZT}}} [Q_{\mathrm{PZT}}] \begin{bmatrix} d_{31} \\ d_{31} \end{bmatrix} dz.$$

The resultant flexural-extensional piezoelectric coupling moments are given by

$$\begin{bmatrix} M_r^P \\ M_\theta^P \end{bmatrix} = \int_{z_{\mathrm{bottom\_PZT}}}^{z_{\mathrm{top\_PZT}}} \frac{V}{h_{\mathrm{PZT}}} [Q_{\mathrm{PZT}}] \begin{bmatrix} d_{31} \\ d_{31} \end{bmatrix} z dz.$$

B. Governing equations of displacement

The integrated resultant equations (9) and (10) are substituted in equilibrium equations (1) and (2) to obtain the governing displacement equations. The resolution of these equations gives the radial displacement $u_0(r)$ and the circumferential displacement $\theta(r)$.[5] Vertical displacement is obtained by the integration of the transverse slope equation $\theta(r)$ $[w(r) = \int_r \theta(r) dr]$, giving

$$w(r) = \begin{cases} \frac{R}{k_0}\left[c_1 I_0\left(k_0 \frac{r}{R}\right) - c_2 K_0\left(k_0 \frac{r}{R}\right)\right] + c_3, & N_0 > 0 \\ \frac{1}{4} c_1 r^2 + c_2 \ln r + c_3, & N_0 = 0 \\ -\frac{R}{k_0}\left[c_1 J_0\left(k_0 \frac{r}{R}\right) + c_2 Y_0\left(k_0 \frac{r}{R}\right)\right] + c_3, & N_0 < 0, \end{cases} \tag{11}$$

where c_1, c_2, and c_3 are constants determined via boundary conditions and interface matching conditions.[5] The three equations $u_0(r)$, $\theta(r)$ and $w(r)$ are valid for the inner and the outer plate but their expressions depend on the sign of the averaging value of the initial stress [Eq. (3)] because of the use of Bessel functions.

C. Buckling effect consideration

The established analytical model uses the same equations as in linear buckling analysis. A structure's buckling occurs when the compressive resultant radial force at the clamped edges $N_r(R_2)$ is higher than the critical radial force $N_r(R_2)_{\mathrm{cr}}$. In our case, buckling effects can thus occur in the annular part clamped along the R_2 radius if compressive forces are applied. The critical radial force was determined by Timoshenko and Gere[15] using linear buckling analysis for a monolayer circular thin plate with clamped edges and a hole at the center. The relationship for a multilayer annular plate was extended and given by

$$N_r(R_2)_{\mathrm{cr}} = k\frac{D_2}{R_2^2}, \tag{12}$$

where k is a numerical factor, depending on the ratio R_1/R_2. Values of k have been determined for various ratios R_1/R_2 and a Poisson ratio of 0.3. D_2 is the equivalent stiffness coefficient and is given by $D_2 = D_{11} - B_{11}^2/A_{11}$ where D_{11}, B_{11}, and A_{11}, are respectively the elements of the $[D]$, $[B]$, and $[A]$ matrices.

D. Analytical model validation and analytical behavior of buckled micromembranes

The analytical model has been exploited in two ways. To determine its accuracy, a first validation step by comparison with a finite element model has been performed within nonbuckling conditions. Second, the analytical model thus validated was extended to the study of buckled micromem-

TABLE II. Material properties used in analytical and finite element models.

Material	Radius (μm)	Thickness h_i (μm)	Young's modulus E_i (Gpa)	Poisson's ratio ν_i	In-plane stress σ_i (MPa)
Platinum[a] (top electrode)	R_1	0.14	145	0.35	500
PZT 54/46[b]	R_1	0.95	96	0.45	100–800
Platinum[a] (bottom electrode)	R_1	0.15	145	0.35	500
Thermal oxide[c]	R_2=200 μm	0.25	70	0.17	−260
Silicon[d]	R_2=200 μm	1.5–5	169	0.3	−15

[a]Branger *et al.* (Ref. 16).
[b]Zakar *et al.* (Ref. 17) and Delobelle *et al.* (Ref. 18).
[c]Kim (Ref. 19).
[d]Dolbow and Gosz (Ref. 20).

branes. Starting point was a plate consisting of two first layers: a silicon base with a thin oxide layer, with a total radius of R_2. Three supplementary layers have been added: a piezoelectric layer (PZT 54/46) with its two platinum electrodes (top and bottom). The radius of this three stack materials is R_1. The properties of the five layers are summarized in Table II. From Eq. (3), the resultant stresses for the inner and outer part are, respectively, tensile and compressive, thus establishing the equation type for the calculation of the vertical deflection, according to Eq. (11).

As the resultant stress is compressive in the outer annular part, the first step consists of determining the buckling point of the micromembranes. Two main parameters may induce buckling effects: the layer thickness and the R_1/R_2 ratio, according to Eq. (12). The buckling point for different values of the silicon thickness and a ratio R_1/R_2 of 0.375 was calculated. The value of k was determined for the R_1/R_2 ratio of 0.375.[15] For the determination of k, the influence of the Poisson ratio of the $Si-SiO_2$ stack was considered to be equal to 0.3, according to the values of Table II. Figure 2 shows the obtained results.

To determine the buckling point, the critical radial force and the resultant radial force at the clamped edge for the annular outer part were calculated, according to Eqs. (12) and (9) respectively. Micromembranes are under buckling

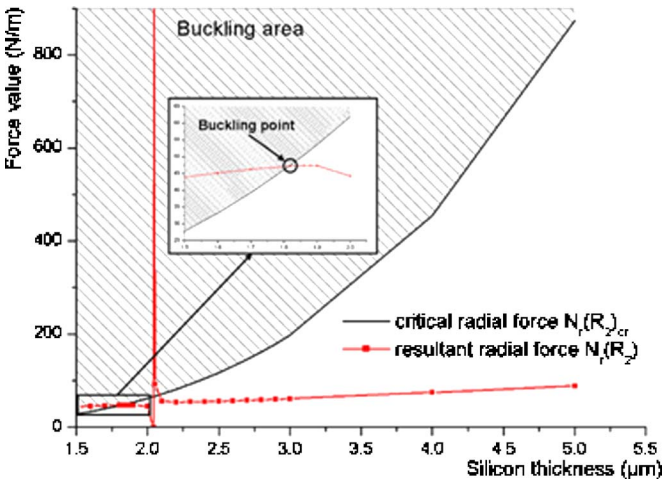

FIG. 2. (Color online) Determination of the buckling point of micromembranes with R_1=75 μm and R_2=200 μm vs silicon thickness.

effects when the resultant radial force is higher than the critical radial force. As depicted in Fig. 2, the buckling point is obtained for a silicon thickness h_{Si} of 1.82 μm and structures will be buckled if the value of h_{Si} is lower than this value. Thus, to verify the accuracy of the analytical model, comparison with finite element models was performed for a value of silicon thickness far from the buckling point. The chosen value was h_{Si}=4 μm.

First of all, for the model's verification, we studied two configurations. The first one is the influence of tensile in-plane stress of PZT on initial deflection. The second one consists of the study of the vertical deflection for different values of R_1/R_2 ratio.

The structure described above has been modelized using COVENTORWARE2005®.[24] Symmetries along the X and Y axes permitted to establish a model based on quarter micromembrane. Approximatively 35 000 parabolic tetrahedric elements were used, but the number varied with geometry. As a qualitative approach, Fig. 3 shows three-dimensional images obtained with analytical model (a) and COVENTORWARE finite element model (b) and the same behavior for the two models was obtained. Figure 4(a) shows a comparison for different values of the in-plane stress of PZT. Z deflection values correspond to the deflection at the center of the plate $w(0)$. The study was made for two cases: R_1/R_2=0.375 and 0.6 for R_2=200 μm. Results are in good agreement with a standard deviation of less than 2%. Close results were also obtained in the study of the R_1/R_2 ratio on the initial deflection for R_2 =200 μm, as shown on Fig. 4(b). FEM and analytical model are in good agreement for $R_1/R_2 \leqslant 0.7$ with a standard deviation of less than 5%.This is due to the higher influence of the inner tensile part with higher radius R_1. Indeed, the approximation for the calculation of the resultant stress for the five layer plate is less preponderant when R_1/R_2 is small. It is nevertheless worth noting that the close results allowed the validation of the accuracy of the analytical model in the range where $R_1/R_2 \leqslant 0.7$.

The validation of the analytical model permitted its use for the design of buckled micromembranes. The vertical deflection was calculated for different values of silicon thickness close to the buckling point according to Fig. 2. The study was performed for an R_1/R_2 ratio of 0.375 with R_2 =200 μm. Figure 5 shows a static profile of buckled mi-

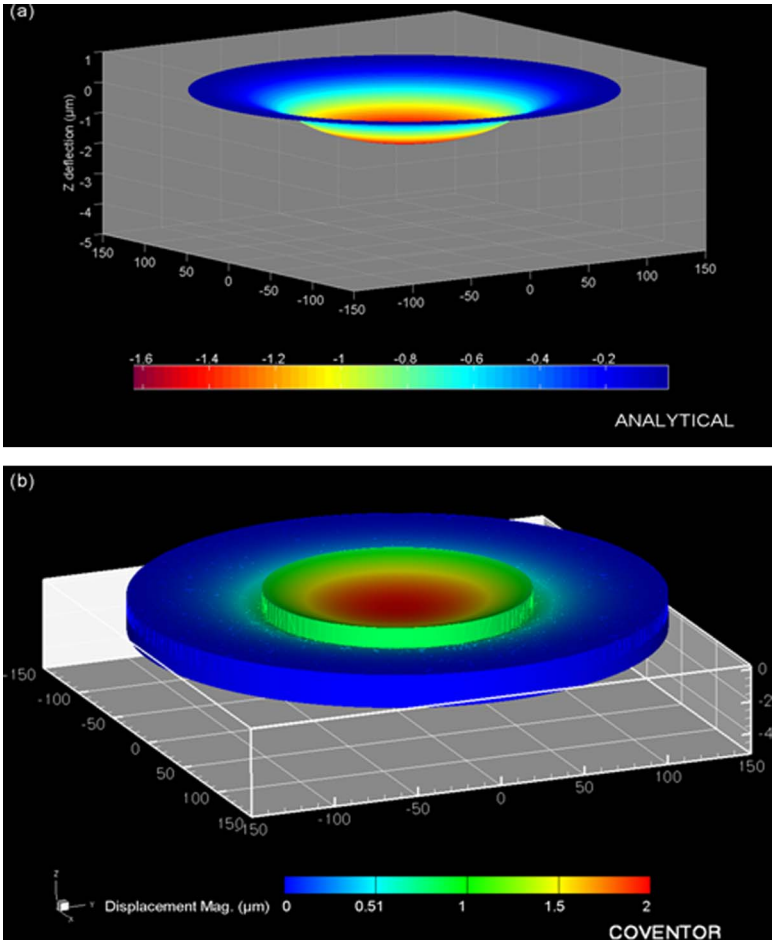

FIG. 3. (Color online) Three-dimensional images of membranes with $R_1=75$ μm and $R_2=200$ μm obtained with (a) analytical model and (b) Coventor finite element model.

cromembrane obtained with the analytical model for $h_{Si}=1.78$ μm. In Fig. 6 the influence of the silicon thickness on the vertical deflection is plotted. Results are in good agreement with the predicted buckling point ($h_{Si}=1.82$ μm) as the vertical deflection at the center is positive and structure is buckled. These results determined the choice of a silicon thickness of 2 μm, a radius R_1 of 75 μm, and a total radius R_2 of 200 μm for the fabrication of buckled micromembranes.

III. FABRICATION AND EXPERIMENTAL SETUP

A. Device fabrication process

4×4 matrices of piezoelectric micromembranes have been fabricated by standard micromachining techniques. Membranes are circularly shaped with a total radius equal to 200 μm. Each micromembrane can be individually actuated through a PZT thin film. This active part is circularly shaped with a radius of 75 μm as shown on Fig. 7.

The main steps of fabrication process are depicted on Fig. 8. The starting substrate is a 100 mm diameter, ⟨100⟩, *N*-type silicon-on-insulator (SOI) wafer, with a 1 μm thick buried oxide and a 2 μm thick top silicon layer (resistivity of 7 Ω cm). The first step consisted of the growth of 50 nm thick thermal oxide on the entire SOI wafer before the sputtering of TiO_2/Pt (10 nm/150 nm) for the bottom electrode. The film was lifted off with a Shipley 1818 photoresist to define circular electrodes with a radius of 75 μm. The 950 nm thick 54/46 $Pb(Zr_xTi_{1-x})O_3$ film was then deposited by rf magnetron sputtering. The 54/46 composition choice is due to its proximity with the morphotropic phase boundary composition ($x=53$), which has the largest piezoelectric and dielectric constants.[21] In most studies, PZT films are deposited at 650 °C. Instead, our PZT film[22] was deposited without intentional substrate heating to allow patterning by lift-off of the PZT film with the Shipley 1818 photoresist. This PZT layer is circularly shaped with a radius 5 μm higher than electrode layers to avoid eventual shortcuts between the top and bottom metallic electrodes. Deposited films were therefore amorphous since temperature rise during deposition does not exceed 150 °C. After resist stripping, a 30 min crystallization annealing at 625 °C was performed. Then, another deposit followed by a lift-off was processed with Ti/Pt (10 nm/140 nm) for top circular electrodes with the same radius as bottom electrode. A passivation silicon oxide film (200 nm thick) was deposited by plasma enhanced chemical vapor deposition (PECVD). Contact pads were then opened by a wet etching of oxide using HF buffer. To finish, the circular membranes (with a total radius of 200 μm) were defined by vertical sidewall etching on the backside of the SOI wafer using the deep reactive ion etching technique. The 1 μm thick SiO_2 acts as an etch stop layer for the dry silicon etching. This layer was then removed using another reactive ion etching process.

Figure 7 shows a close-up view of two membranes with a radius of 75 μm for PZT layer. As shown in this figure, the

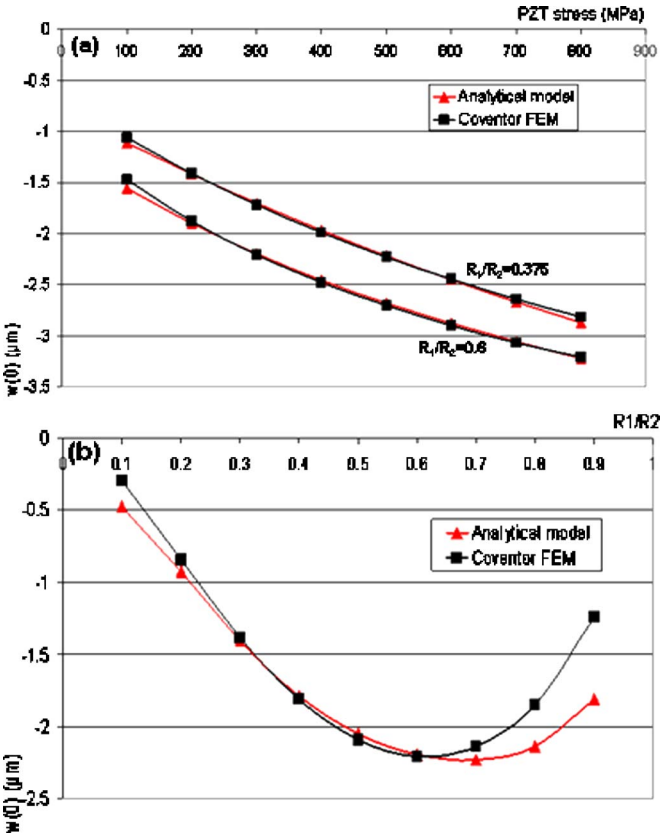

FIG. 4. (Color online) Comparison of analytical model and Coventor finite element model for a five layer micromembrane with $R_2=200$ μm. (a) Influence of PZT in-plane stress on vertical deflection at the center of plate for $R_1/R_2=0.375$ and 0.6. (b) Influence of R_1/R_2 ratio on vertical deflection at the center of plate with $\sigma_{PZT}=300$ MPa.

circular geometry of micromembranes is clearly defined. All membranes are connected with a common ground plane through bottom electrodes. The top electrode allows the individual actuation of the membranes.

B. Dual-beam interferometer

A ZoomSurf 3D© (Fogale Nanotech, Nîmes, France) dual-beam interferometer has been used for measurements of static deflection of the fabricated micromembranes. Optical dual-beam interferometer has been described in detail elsewhere.[23]

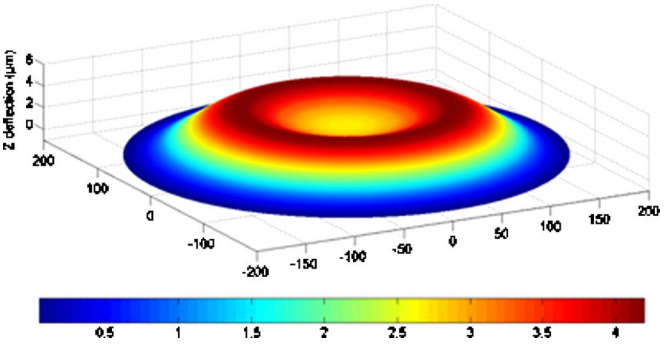

FIG. 5. (Color online) Three-dimensional image of a five layer buckled membrane with $R_1=75$ μm, $R_2=200$ μm, and $h_{Si}=1.78$ μm obtained with analytical model.

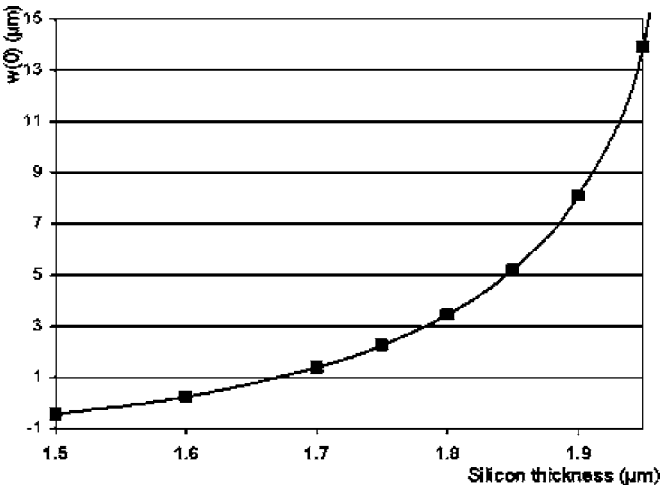

FIG. 6. Influence of the silicon thickness on the vertical deflection of buckled micromembranes with $R_1=75$ μm and $R_2=200$ μm.

Briefly, this system is based on a standard optical microscope with an interferometric objective. It is equipped with two light sources: a tungsten-halogen white source for large displacements and a quasimonochromatic red source for small deflections and dynamic measurements. As depicted in Fig. 9, incident light beams are separated via a separating cube between the sample surface and an internal reference mirror. Interference fringes, resulting from reflected beams from the reference mirror and the sample surface, are recorded via a Standard charge-coupled device (CCD) monochromatic camera. An automatic treatment by Fourier transform of the recorded interferogram permits the topography of the sample's surface to be obtained via the FOGALE 3D software. This completely automated noncontact technique gives measurements with a vertical resolution down to 0.1 nm. Typical two-demensional (2D) topography of a micromembrane is shown on Fig. 10(a), and a three-dimensional (3D) profile of two similar membranes is shown on Fig. 10(b).

IV. RESULTS AND DISCUSSION

A. Static deflection measurements of microstructures

Measurements were made in static mode with the tungsten-halogen white source of the aforementioned interferometer because of the large deflection values of the devices.

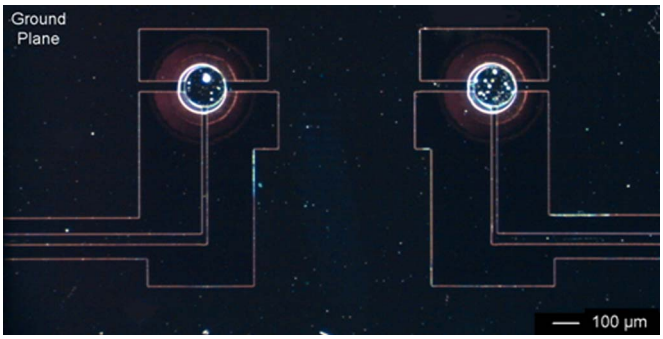

FIG. 7. (Color online) Optical microscope image of two fabricated circular micromembranes with radii $R_1=75$ μm and $R_2=200$ μm.

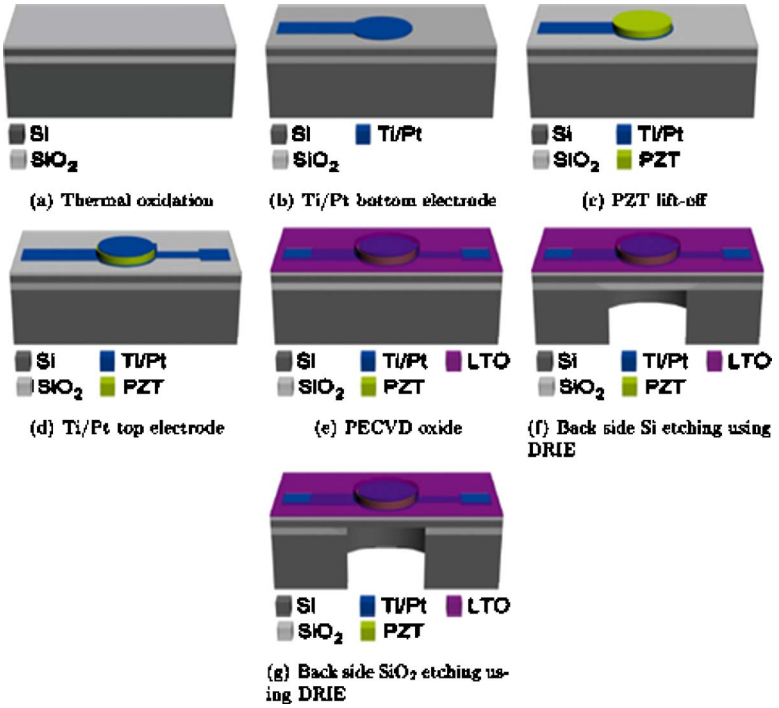

FIG. 8. (Color online) Fabrication steps of clamped piezoelectric circular micromembranes.

The displacement of the microstructure was directly measured by applying a static potential in the range of −18–+18 V between top and bottom platinum electrodes. The induced electric field in the PZT thin film along the Z axis changed the deflection of the structure due to the reverse piezoelectric effect. First, Fig. 10 shows the 3D profile of two fabricated micromembranes with $R_1=75$ μm and $R_2=200$ μm. This figure shows that a buckling profile was obtained on the fabricated micromembranes as predicted by the analytical model. As the deep reactive ion technique was a critical step of microfabrication, it induced a partial etching of the backside of top silicon layer. Measured thickness varied from 1.75 to 1.85 μm. These values were close to the buckling point defined by analytical model, and measured vertical deflections described in Fig. 11 were in the same range as analytical values depicted in Fig. 6. It is worth noting that titanium layers were neglected in the analytical model as their thickness was insignificant compared to the other layers.

After polarizing the PZT thin film at 18 V for 15 min, dc voltage was changed from +18 to −18 V in both ways with a step of 1 V. Measurements were made 1 min after chang-

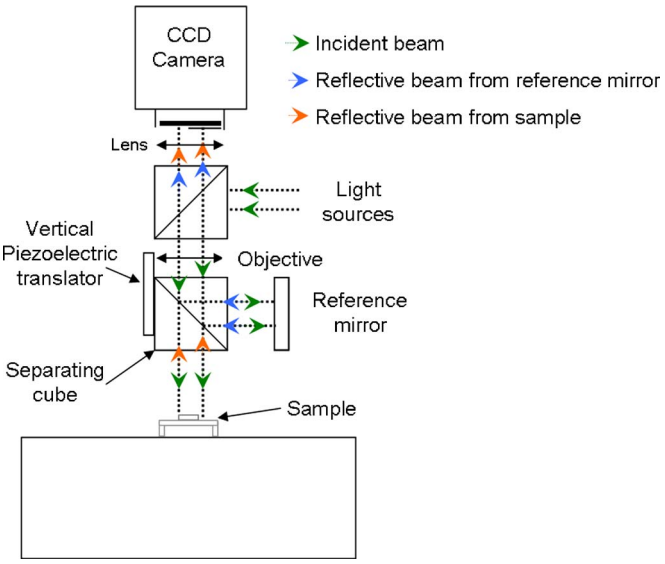

FIG. 9. (Color online) Scheme of dual-beam interferometer optical configuration.

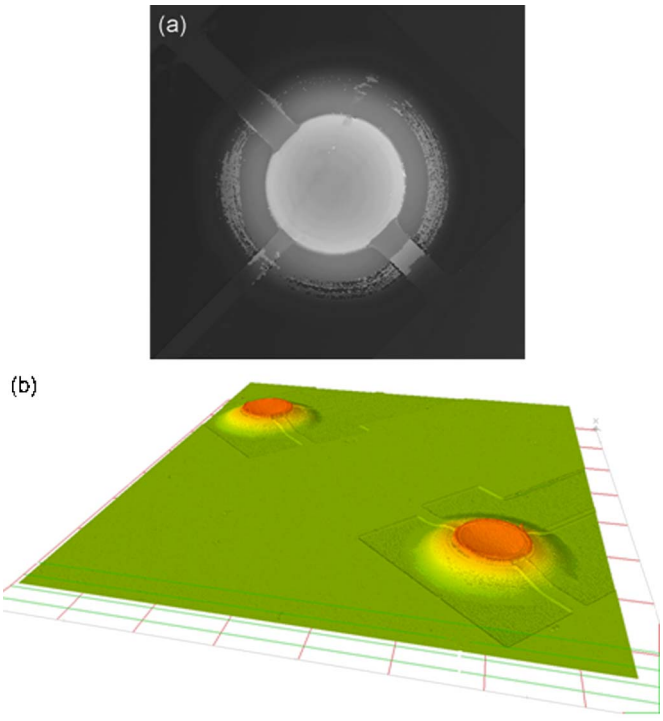

FIG. 10. (Color online) Typical topographies of micromembranes with $R_1=75$ μm and $R_2=200$ μm obtained with a Fogale© interferometer: (a) top view and (b) 3D profile.

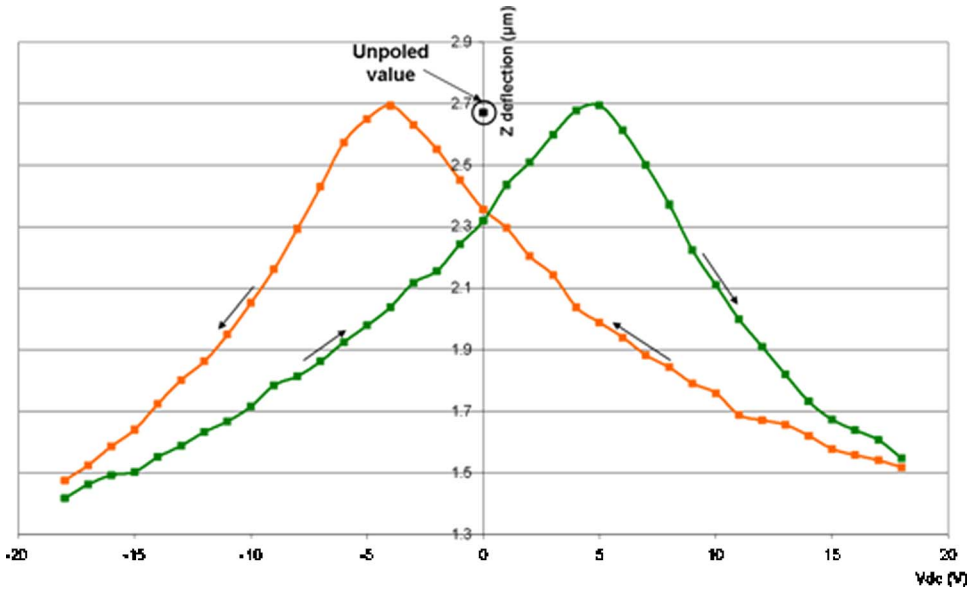

FIG. 11. (Color online) Influence of dc voltage on the vertical deflection of fabricated micromembrane with $R_1=75\ \mu$m and $R_2=200\ \mu$m.

ing the value of the dc bias. This time's value was calibrated taking into account the stabilization of structure for the dc bias under influence of the remanent piezoelectricity. After measurement, microstructures were kept under dc value until equilibrium state was reached. Figure 11 shows an example of the deflection curve. It corresponds to the deflection at the center of the structure for $R_1=75\ \mu$m and $R_2=200\ \mu$m, where the thickness of top electrode, PZT, and bottom electrode stack is subtracted. It shows a large displacement hysteresis with two maximum peaks: −4 and +5 V. These values are close to the coercive field[8] for PZT 54/46 thin films, and deflection for these values is close to the deflection of unpoled membrane. The difference is due to initial internal polarization appearing during the fabrication process and inducing a small variation of deflection of unpoled membrane. The close deflections indicate that after domains were well oriented in high potential values, changes in their orientation for lower values occur and induce the strain relaxation of the PZT thin film until a maximum value of deflection that corresponds to the same behavior as the one for unpoled film, which is the zero piezoelectric strain point.

B. Study of the transverse piezoelectric coefficient d_{31}

In general cases, the determination of d_{31} or e_{31} is made with the dynamic excitation of the piezoelectric film and a dc value equal to 0 V because of remanent piezoelectricity.[7,8,10] In our case, d_{31} calculation is made in static mode with the measurement of deflection with a small variation of the dc value, permitting the measurement of the remanent piezoelectric state. This way of determination is successful, as the analytical model takes into account stress induced by the polarization of PZT thin film.

The generic behavior of the analytical model allowed its modification for a direct calculation of the transverse piezoelectric coefficient d_{31} for buckled membranes. Indeed, for a resultant tensile stress in the inner part of the plate, the modification of Eq. (11) for the variation Δw of the static deflection at the center of the structure induced by a small variation ΔV of dc bias gives

$$d_{31}=\frac{\Delta w}{\Delta V}\frac{1}{K}, \tag{13}$$

where K is a numerical constant determined by the static deflection of the unpoled structure.

The first step thus consisted of the calibration of the analytical model with unpoled buckled membrane for the determination of constant K. For convenience, the 200 nm PECVD oxide is considered as a stack layer above thermal oxide in the analytical model. The calibration is made by adjusting material properties. Changes of only ±10% from the initial value described in Table II are necessary to obtain close values between the analytical model and the fabricated micromembranes. This indicates that analytical model is representative of static the behavior of buckled micromembranes and validates its modification for the calculation of d_{31} from measurements.

Then, measurements of the vertical deflection of the fabricated structures permitted the calculation of variation of deflection Δw at the center for a potential variation ΔV of 1 V. Substitution of Δw and ΔV in Eq. (13) gives the value of d_{31} for each dc bias value. Figure 12 shows the obtained curve of d_{31} vs V_{dc} of PZT 54/46 thin film in range of −18–+18 V. Measurements and calculation were repeated on three micromembranes with geometry parameters equal to $R_1=75\ \mu$m and $R_2=200\ \mu$m. Figure 12 shows a hysteresis-like cycle of d_{31} with excellent values. $|d_{31}|$ shows a strong dependence on applied voltage with large variations from 30 pm/V in high potential values to 75 pm/V around ±8 V, depending on the way the potential is applied. So large variations of d_{31} may be due to the off-axis motion of domains such as the reorientation of 90° domains, superimposed on the lattice motion. These results are in good agreement with literature.[7–10] It also should be noted that the d_{31} value is 0 pm/V when V_{dc} is close to ±4 V, which corresponds to the coercive field. These results are in good agreement with the

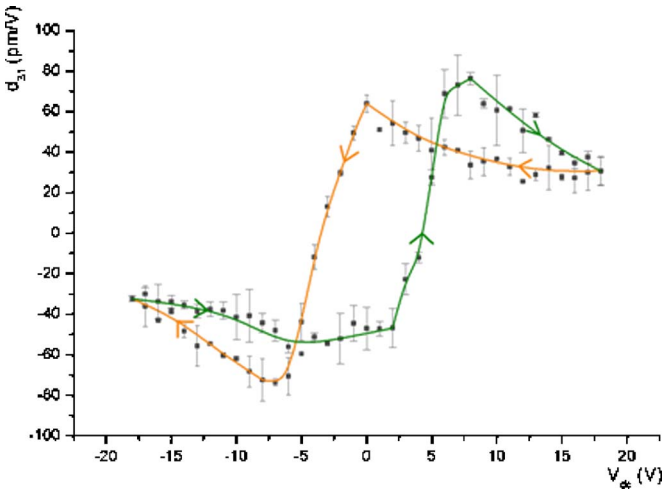

FIG. 12. (Color online) Influence of dc voltage on the piezoelectric constant d_{31} of PZT 54/46 thin film.

maximum of deflection that corresponds to the zero piezoelectric strain, as d_{31} represents the proportional constant of the piezoelectric strain generated by the transverse electric field. Thus, a strong influence of the transverse electric field on the piezoelectric constant d_{31} has been demonstrated with size reduction from millimeter to micrometer on buckled structures.

V. CONCLUSION

In this study, a powerful analytical model for a multilayer circular plate, taking into account the tensile/compressive initial stress of materials, was developed. This model was modified for the study of the piezoelectric constant d_{31} of PZT 54/46 thin film integrated on microscaled circular buckled membranes. It also allowed the demonstration of the strong influence of dc voltage on the value of d_{31} for micromachined PZT. A hysteresislike cycle was obtained with large variations of the coefficient, from ±30 to ±75 pm/V.

The aim of this study was a first step of characterization of the micromembranes in order to determine optimal working conditions. This characterization work was essential because the future use of the microstructures is the development of precise biological assays in dynamic mode with a complete integration of actuation and detection, using the microgravimetric effect.

[1] P. Lugienbuhl, S. D. Collins, G.-A. Racine, M.-A. Grétillat, N. F. D. Rooij, K. G. Brooks, and N. Setter, J. Microelectromech. Syst. **6**, 337 (1997).
[2] P. Muralt, A. Kholkin, M. Kohli, T. Maeder, and N. Setter, Microelectron. Eng. **29**, 67 (1990).
[3] M. Guirardel, L. Nicu, D. Saya, Y. Tauran, E. Cattan, D. Remiens, and C. Bergaud, Jpn. J. Appl. Phys., Part 2 **43**, L111 (2004).
[4] L. Nicu *et al.*, Sens. Actuators B **110**, 125 (2005).
[5] G. Wang, B. V. Sankar, L. N. Cattafesta, and M. Sheplak, Proceeding of ASME International Mechanical Engineering Congress, 2002 (unpublished).
[6] E. Hong, S. Trolier-McKinstry, R. Smith, S. V. Krishnawamy, and C. B. Freidhoff, IEEE Trans. Ultrason. Ferroelectr. Freq. Control **53**, 697 (2006).
[7] M.-A. Dubois and P. Muralt, Sens. Actuators, A **77**, 5810 (1999).
[8] E. Cattan, T. Haccart, and D. Remiens, J. Appl. Phys. **86**, 7017 (1999).
[9] J. F. Shepard, F. Chu, I. Kanno, and S. Trolier-McKinstry, J. Appl. Phys. **85**, 6711 (1999).
[10] I. Kanno, H. Kotera, and K. Wasa, Sens. Actuators, A **107**, 68 (2003).
[11] S. P. Timoshenko and S. W. Krieger, *Theory of Plates and Shells* (McGraw-Hill, New York, 1959).
[12] M. Sheplak and J. Dugundji, J. Appl. Mech. **65**, 107 (1998).
[13] S. A. N. Prasad, B. V. Sankar, L. N. Cattafesta, S. Horowitz, Q. Gallas, and M. Sheplak, Proceedings of AIAA Structures, Structural dynamics and Materials Conference, 2002 (unpublished).
[14] L. Yao, L. Lu, Z. Wang, W. Zhu, and Y. Dai, IEEE Trans. Ultrason. Ferroelectr. Freq. Control **50**, 1262 (2003).
[15] S. P. Timoshenko and J. M. Gere, *Theory of Elastic Stability* (McGraw-Hill, New York, 1963).
[16] V. Branger, V. Pelosin, K. F. Badawi, and P. Goudeau, Thin Solid Films **275**, 22 (1996).
[17] E. Zakar, M. Dubey, R. Polcawich, B. Piekarski, R. Piekarz, J. Conrad, and R. Widuta, Proceedings of MRS Fall Meeting, 1999 (unpublished).
[18] P. Delobelle, O. Guillon, E. Fribourg-Blanc, C. Soyer, E. Cattan, and D. Remiens, Appl. Phys. Lett. **85**, 5185 (2004).
[19] M. T. Kim, Thin Solid Films **283**, 12 (1996).
[20] J. Dolbow and M. Gosz, Mech. Mater. **23**, 311 (1996).
[21] B. Jaffe, W. Cook, and H. Jaffe, *Piezoelectric Ceramics* (Academic, New York, 1971).
[22] B. Jaber, D. Remiens, E. Cattan, P. Tronc, and B. Thierry, Sens. Actuators, A **63**, 91 (1997).
[23] A. Bosseboeuf *et al.*, Proceedings of SPIE Microsystems, Metrology and Inspection Congress, 1999 (unpublished).
[24] COVENTORWARE 2005, Coventor, Inc., 4001 Weston Parkway, Cary, NC 27513.